Optical Materials 136 (2023) 113466

Contents lists available at ScienceDirect

Optical Materials

journal homepage: www.elsevier.com/locate/optmat

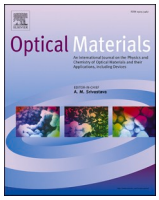

Research Article

Tunability of nonlinear optical properties of amorphous Cu–Al–O films induced by thermal oxidation

Jingjing Xu [a], Qingyou Liu [b], Xiao Li [c], Ruijin Hong [a,*], Chunxian Tao [a], Qi Wang [a], Hui Lin [a], Zhaoxia Han [a], Dawei Zhang [a]

[a] Engineering Research Center of Optical Instrument and System, Ministry of Education and Shanghai Key Lab of Modern Optical System, University of Shanghai for Science and Technology, No.516 Jungong Road, Shanghai, 200093, China
[b] Key Laboratory of High-temperature and High-pressure Study of the Earth's Interior, Institute of Geochemistry, Chinese Academy of Sciences, Guiyang, 550081, China
[c] Department of Physics, Beijing Technology and Business University, Beijing, 100048, China

ARTICLE INFO

Keywords:
Cu/Al alloy
Magnetron sputtering
Anneal
Nonlinear conversion

ABSTRACT

A series of Cu–Al–O thin films with excellent nonlinear absorption properties were prepared by magnetron sputtering at room temperature. An absorption peak at around 440 nm was observed in the as-deposited thin films, with $CuAlO_2$ as the main phase. After thermal oxidation at 400 °C, the surface roughness of the films decreased, the absorption peak was blue-shifted, with the optical band gap increased. Open aperture Z-scan measurements revealed that the as-deposited samples had strong saturable absorption and reached the maximum nonlinear absorption coefficient (β) of -6.29×10^{-5} cm/W. The nonlinear optical conversion from saturable absorption to reverse saturable absorption was observed in as-annealed samples with β values up to 2.592×10^{-5} cm/W. In addition, the time-domain finite-difference simulation results were basically consistent with those of the experimental results.

1. Introduction

Transparent conductive oxides (TCOs) have become one of the research hotspots in the field of optoelectronics in recent years due to their high conductivity and transmittance in the visible light region [1,2], widely used in solar cells, flat panel displays, light-emitting diodes, electromagnetic shielding and touch panels [3,4]. For a long time, the production and application of TCOs mainly focus on ITO, AZO, FTO and so on. The research and development of novel TCOs by researchers from all over the world have never stopped.

In 1997, Kawazoe et al. [1] first reported in Nature, which aroused global attention to the new transparent conductive oxide $CuAlO_2$ and set off a research boom. Since then, some novel TCOs such as LaCuOS, $CuGaO_2$, $CuCrO_2$ were proposed by substitution doping. In order to optimize the preparation process to improve the conductivity of $CuAlO_2$, so far, the reported preparation methods mainly include pulsed laser deposition [5], sputtering deposition [6], sol-gel [7], solid-phase synthesis [8], vapor deposition [9], etc. Compared with other preparation techniques, magnetron sputtering has the advantages of fast deposition speed, good density, good uniformity and so on, which can be applied to large-scale deposition. In 2014, Ping-Hung Hsieh et al. [10] reported the effect of different sputtering power on the growth of $CuAlO_2$. Furthermore, high temperature annealing is the decisive step in the formation of $CuAlO_2$ thin films [11–13], which is the most commonly used post-treatment method. In recent years, most of the reports on $CuAlO_2$ thin films are doping, fine preparation and post-processing to improve thermoelectric properties, optimize optical properties, accelerate crystallization and improve purity [14,15]. However, the research on the nonlinear optical properties of $CuAlO_2$ has not been reported yet.

Nonlinear optics (NLO) plays an important role in the study of the interaction between light and materials. Z-scan technology has been widely used because of its simple device and high sensitivity, and it can separate the nonlinear absorption coefficient (β) and the nonlinear refractive index [16]. Nonlinear absorption (NLA) includes two effects: saturable absorption (SA) and reverse saturable absorption (RSA), which compete with each other. In previous reports, it has been observed a nonlinear optical phenomenon of switching from SA to RSA in different materials [17,18]. We believe that it is necessary to investigate the nonlinear optical properties of $CuAlO_2$, which is of great significance for its applications in optical switching, optical limiting and other fields.

* Corresponding author.
E-mail address: rjhong@usst.edu.cn (R. Hong).

https://doi.org/10.1016/j.optmat.2023.113466
Received 18 October 2022; Received in revised form 23 December 2022; Accepted 10 January 2023
Available online 20 January 2023

In this work, we prepared Cu–Al–O thin films by magnetron sputtering, followed by thermal treatment. The nonlinear optical properties of the films before and after thermal treatment were investigated by the open aperture (OA) Z-scan method, and the nonlinear absorption coefficients (β) were further estimated.

2. Experimental

Cu–Al–O thin films were prepared on soda-lime glass by magnetron sputtering at room temperature. The sputtering target was copper–aluminum (50/50 at%) alloy with a purity of 99.99% and the sputtering gas was high purity argon (99.99%). Before sputtering, the substrates were cleaned in acetone, ethanol and deionized water for 15 min, then dried in air sequentially. The target was bombarded with argon ion for 10 min to remove the oxides on the surface. The base pressure and working pressure were 5×10^{-4} Pa and 6×10^{-1} Pa, respectively [19]. In this experiment, the deposition time of all samples was set to 45 s and the sputtering power was 50 W, 75 W, 100 W, 125 W and 150 W, respectively. Meanwhile, the deposited samples were marked as sample 1 (S1), sample 2 (S2), sample 3 (S3), sample 4 (S4), and sample 5 (S5) in turn. Subsequently, the as-deposited films were placed in a thermal oxidation furnace at 400 °C for 2 h. The as-annealed films were labeled as sample 1' (S1′), sample 2' (S2′), sample 3' (S3′), sample 4' (S4′), sample 5' (S5').

The morphology and crystal structure of the thin films were characterized by atomic force microscopy (AFM: XE-100, Park System) and X-ray diffraction (XRD: Bruker AXS/D8 Advance system). The optical properties of the samples were studied by the UV–vis–NIR double-beam spectrophotometer (Lambda 1050, PerkinElmer, USA) with a wavelength range of 200 nm–2000 nm. Further determination of chemical composition and valence state of samples used the Thermo Scientific K-Alpha þ X-ray photoelectron spectroscopy (XPS). Properties of the third order NLO were investigated by the open aperture (OA) Z-scan system (T-Light, Menlo Systems), which have a mode-locked picosecond laser with a wavelength of 1550 nm, a duration of 2 ps and a repetition rate of 100 MHz as the optical excitation source which is focused through a 15 mm lens, and the detector receives the signal. All the measurements were carried out at room temperature.

3. Results and discussion

3.1. Structure and surface topography

Fig. 1 shows the XRD patterns of the as-deposited and as-annealed samples. Obviously, a broad peak around 22° in the figure is related to the glass substrate. No other diffraction peaks are observed in the as-deposited samples (Fig. 1(a)), indicating that the deposited films were amorphous. In the vacuum environment, films were naturally oxidized due to the heat generated by the sputtering process. In addition, Reddy et al. [20] reported that Cu–Al–O films formed at room temperature were intrinsically amorphous because there was not enough thermal energy for adatoms to diffuse and nucleate on the substrate surface. Similar results were also reported by Chen et al. [13]. According to Fig. 1 (b), the samples were still amorphous after 400 °C heat treatment, because the annealing temperature was not enough to promote the crystallization of $CuAlO_2$ phase. As reported by Panthawan et al. [21], no significant peak was observed at the annealing temperature lower than 400 °C. The Cu–Al–O phase was amorphous after annealing at 500 °C, and the $CuAlO_2$ phase appeared only when the annealing temperature increased to 600 °C [22,23].

The surface morphology of Cu–Al–O thin films before and after thermal oxidation was analyzed by AFM, as shown in Fig. 2(a-f). It can be obtained from Fig. 2(a-c) that the root mean square (RMS) surface roughness of as-deposited samples (S1–S3) are 371.965 p.m., 322.855 p.m., and 230.52 p.m., respectively. The results show that the as-deposited Cu–Al–O films have good uniformity, and the density and smoothness of the films increase with the increase of sputtering power. Thermal treatment improved the surface energy of the film, enhanced the diffusion and migration of surface atoms, and improved the surface defects. Therefore, the as-annealed film became smoother and the RMS surface roughness decreases. From the line graph in Fig. 2(g), we can clearly observe the effect of thermal treatment on the surface roughness of samples. The surface roughness of the as-deposited films is negatively correlated with the increase of the deposition power, and the surface roughness of the films decreases in different degrees after thermal treatment. For example, the root mean square surface roughness of the S2 is 322.855 p.m., which decreases to 295.354 p.m. after thermal oxidization.

3.2. Composition and optical properties

Fig. 3 presents the XPS spectra of Cu–Al–O films before and after thermal treatment (S1–S3 and S1′-S3′). According to Fig. 3(a), the XPS spectra of all samples in the scanning range of 0–1200 eV confirm the successful preparation of Cu–Al–O films. All XPS high-resolution spectra were charge-corrected with the C 1s peak at 284.8 eV as reference. Fig. 3 (b-c) reveals the Cu 2p core energy spectra of the Cu–Al–O film. Each sample has two strong peaks at 931.83 eV and 951.71 eV, which correspond to Cu 2p 3/2 and Cu 2p 1/2 of the $CuAlO_2$ phase, respectively [14,24]. In addition, the two weak peaks at 933.77 eV and 954.04 eV are attributed to Cu 2p 3/2 and Cu 2p 1/2 of CuO [25]. Although Cu^{2+} ions are detected, no obvious (quite weak) satellite peak signal is observed due to its low content. To sum up, we successfully prepared $CuAlO_2$ thin films at room temperature, but it was difficult to obtain pure $CuAlO_2$ due to the complicated preparation environment [26]. In the high-resolution Al 2p XPS spectrum (Fig. 3(d-e)), three peaks obtained by deconvolution belong to Al^0 (at 72.1 eV), Al_2O_3 (at 74.23 eV) and Al_2O_x/Al (at 76.54 eV) in sequence. After thermal treatment, Al atoms in S1–S3 were fully oxidized, and the ratio of defective Al_2O_x/Al was significantly reduced. As shown in Fig. 3(f), the peak of lower

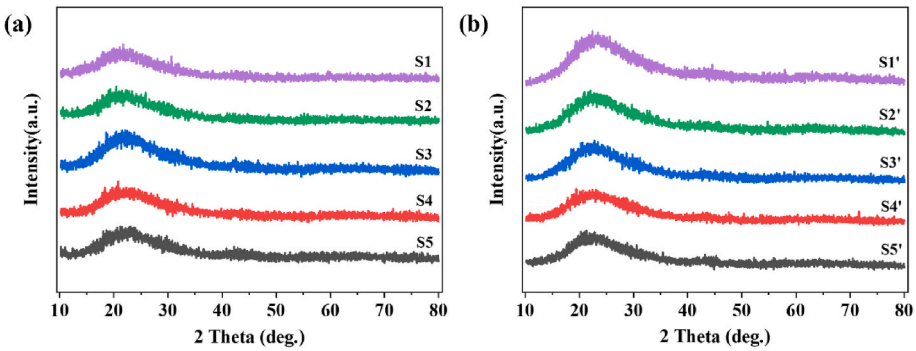

Fig. 1. XRD patterns of **(a)** as-deposited Cu–Al–O films and **(b)** as-annealed films.

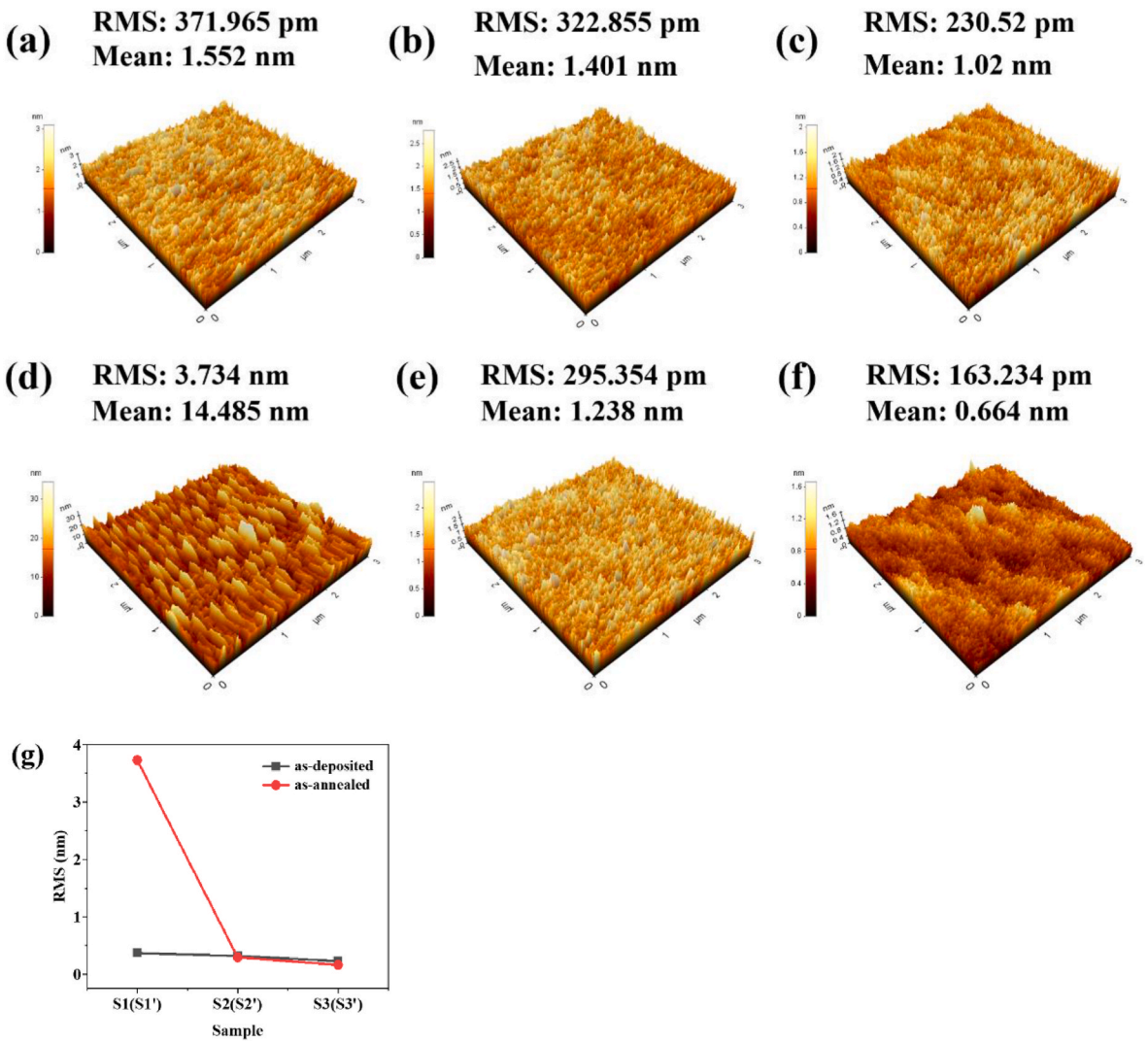

Fig. 2. Atomic force microscopy images of sample S1–S3 **(a–c)** and S1′-S3' **(d–f)**; **(g)** Variation of RMS surface roughness of samples before and after thermal oxidation.

binding energy (at 530.7 ± 0.3 eV) in the O 1s spectra corresponds to oxygen vacancies (interstitial oxygen), and the peak of higher binding energy (at 531.6 ± 0.3 eV) corresponds to the Al–O bond in $CuAlO_2$ [11,27,28]. Fitting analysis showed that the percentage of interstitial oxygen in samples S1–S3 was 44.4%, 30.28% and 38.3%, respectively. After thermal oxidation, the oxygen vacancy content increased to different degrees, and its proportions were 54.61%, 62.2% and 61.64% respectively, which was caused by the introduction of defects caused by heat treatment and the change of the surface structure of the films [29]. These defects and oxygen vacancies could be used to explain the variation of the third order nonlinear characteristics of the samples [30].

To further investigate the optical properties of the samples, the UV–Vis absorption spectra in the range of 200–2000 nm was measured, as shown in Fig. 4. A sharp absorption edge is detected in the as-deposited samples (Fig. 4(a)) at a wavelength of about 330 nm, corresponding to a peak position of approximately 440 nm, which is consistent with previous reports [31–33]. Obviously, the characteristic absorption peak intensity of $CuAlO_2$ increases with the increase of sputtering power. After thermal treatment, the characteristic absorption peak at 440 nm is blue-shifted to around 400 nm, and the absorbance of all samples decreased significantly. This may be due to the significant reduction of Cu content in the film after annealing (see Fig. 3), the Cu/Al ratio decreased, which causes the shift of the optical absorption edge to the shorter wavelength region [12]. At the same time, the band-edge blue-shift of the as-annealed films is also attributed to the widening of the band gap, as discussed later. Notably, a broad absorption band belonging to the phase of CuO appears at the wavelength of 870 nm [34,35].

The fundamental absorption, which corresponds to the electron excitation from the valence band to the conduction band, has been widely used to determine the optical bandgap of semiconductor materials. The relationship between the optical absorption coefficient (α) and the photon energy ($h\nu$) can be expressed as [36]:

$$(\alpha h\nu)^n = A(h\nu - E_g)$$

Where A is a constant, α is the absorption coefficient, $h\nu$ is the incident photon energy, and E_g is the optical bandgap. The exponent n depends on the type of transition, n = 2 and n = 1/2 for direct and indirect transition, respectively [37]. The linear portion of the $(\alpha h\nu)^{1/2}$ versus $h\nu$ curve in Fig. 5 is extrapolated to $\alpha = 0$ to estimate the optical bandgaps of all samples. It can be seen from Fig. 5(a) that with the increase of sputtering power, the E_g of the as-deposited Cu–Al–O film decreased from 3.58 eV to 3.02 eV. The optical band gap of all films increased after thermal treatment in Fig. 5(b) and was estimated to be 3.74–3.22 eV. Thermal oxidation induced the increase of oxygen vacancy, the increase of carrier concentration, which widened the band gap of the

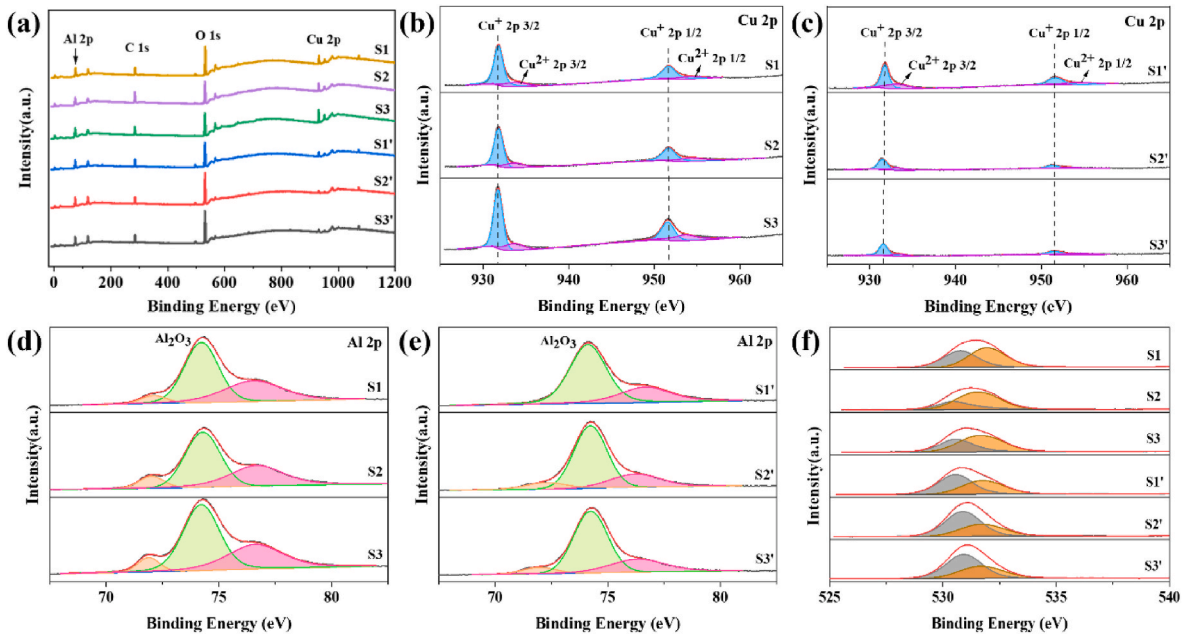

Fig. 3. (a) Full-range XPS spectra; Cu 2p spectrum of samples before **(b)** and after **(c)** thermal treatment, **(d–e)** Al 2p spectrum, and **(f)** O 1s spectrum of all tested samples.

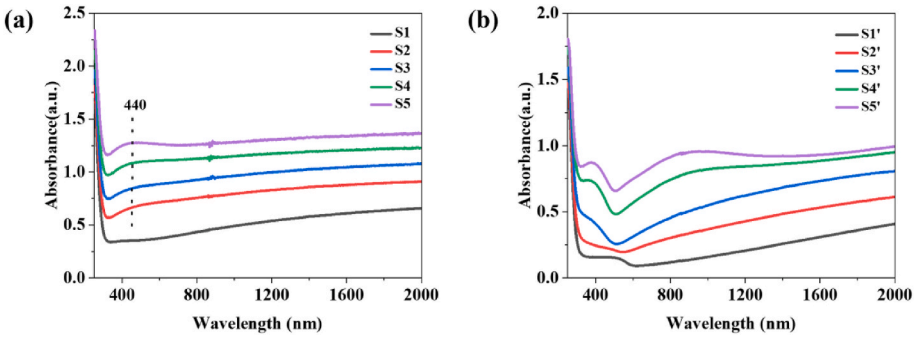

Fig. 4. Optical absorption spectra of **(a)** as-deposited Cu–Al–O films and **(b)** as-annealed samples.

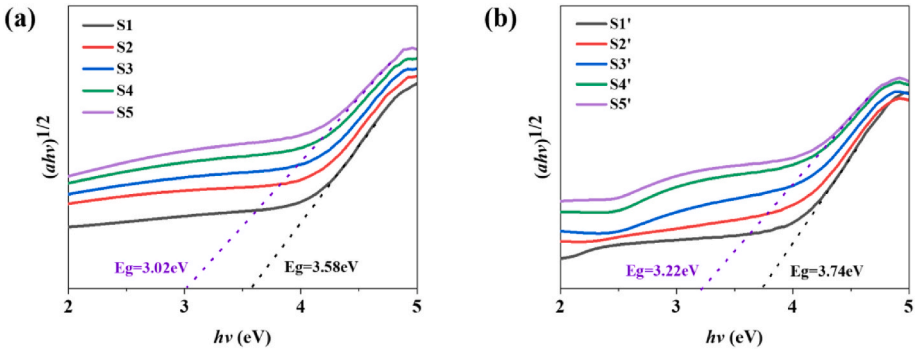

Fig. 5. Optical band gaps of all samples before **(a)** and after **(b)** thermal treatment.

semiconductor as the absorption edge rose to a higher energy state (blue-shifted). M. Nisha et al. [38] reported that the increase of the band gap with the carrier concentration can be explained by the Burstein–Moss effect [39]. Here, we consider that the shift of band gap is also related to the corresponding change in transmittance and particle size [40].

3.3. Nonlinear optical (NLO) properties

The third-order nonlinear absorption properties of Cu–Al–O thin films were characterized by an open aperture Z-scan system with an excitation wavelength of 1550 nm and an excitation energy of 3.1 × 10^{-3} GW/cm^2 [41]. Fig. 6(a) shows the open aperture Z-scan transmittance curves of Cu–Al–O films prepared with different sputtering

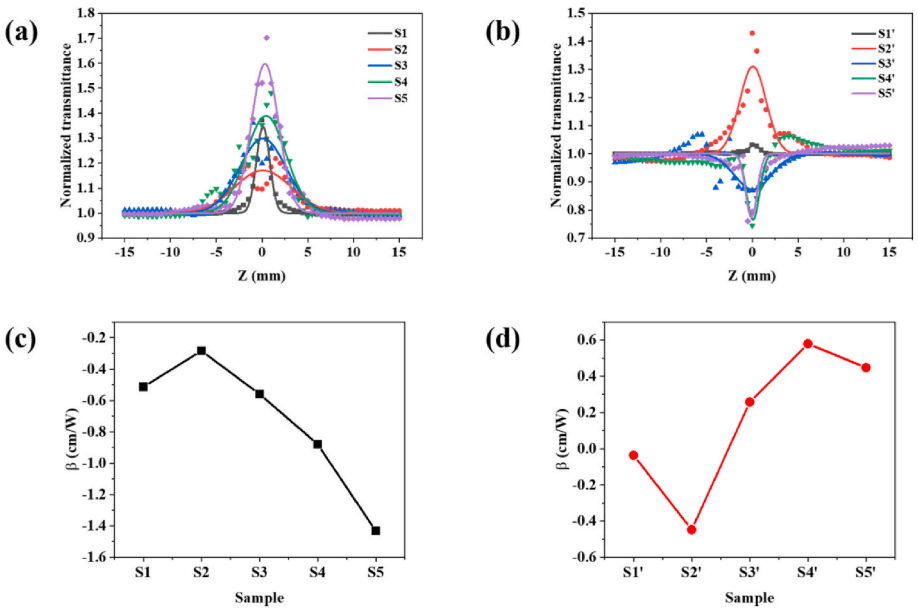

Fig. 6. The open aperture (OA) Z-scan transmittance curves of **(a)** as-sputtered and **(b)** thermally treated Cu–Al–O thin films at 1550 nm wavelength; **(c–d)** The nonlinear absorption coefficient (β) of the films.

powers. It can be seen that the open aperture Z-scan transmittance curves of as-deposited samples (S1–S5) are peak, showing strong saturable absorption (SA). When the sputtering power is low, S1 exhibits a strong peak intensity of saturated absorption, which may be due to the enhanced interaction between the light and the material with thinner layer [42]. After that, the sputtering power is increased to 75 w, and the peak intensity of nonlinear transmission of thin films increases with the increase of sputtering power (S2–S5 in Fig. 6(a)). The nonlinear transmission curves of the as-annealed samples are plotted from the Z-scan data, as shown in Fig. 6(b). It can be seen that the saturation absorption peak of S1' decreases significantly compared with that before thermal treatment, which may be due to the great influence of thermal oxidization on the thickness of low-power sputtering samples. The normalized transmittance of S2' has a certain increase compared with that of as-deposited S2. It is worth noting that the open-aperture Z-scan transmittance curves of S3', S4', and S5' are valley, indicating that the nonlinear absorption mechanism of the Cu–Al–O film is transformed from SA to RSA (reverse saturable absorption) [43]. In semiconductors, the RSA effect is mainly caused by two-photon absorption (TPA), free carrier absorption (FCA), nonlinear scattering, or a combination of these processes [44].

The value of the nonlinear absorption coefficient (β) is determined based on normalized fit results. For nonlinear absorbing materials, the total absorption under strong excitation consists of two parts: linear absorption (α_0) and nonlinear absorption (β), its simple relationship is: $\alpha = \alpha_0 + \beta I$, where α_0 is the linear absorption coefficient, β is the nonlinear absorption coefficient and I is the laser intensity [45]. The normalized transmittance T_{Norm} is calculated from the following equation [46,47]:

$$T_{Norm} = 1 - \frac{\beta I_0 L_{eff}}{2\sqrt{2}\left[1+\left(\frac{z}{z_0}\right)^2\right]}$$

Here, $L_{eff} = (1 - \exp(-\alpha_0 L))/\alpha_0$ is the effective thickness of the sample, $\alpha_0 = -(1/L)\ln T_L$, L is an actual thickness of the sample and T_L is a linear transmittance of the sample; I_0 is the laser intensity at the focus ($z = 0$); z is the straight-line distance from the sample to the focus and z_0 is the diffraction length of the beam. In Fig. 6(c-d), the nonlinear absorption coefficient β of all samples was plotted into a broken line diagram. The β values for the as-deposited samples (in Fig. 6(c)) are all negative, corresponding to the SA effect. With the increase of sputtering power, the absolute value of β showed an increasing trend, reaching a maximum value of -6.29×10^{-5} cm/W at 150 w (S5). Except for S2', the saturable absorption of other samples is suppressed to varying degrees, and gradually converts to RSA with the increase of sputtering power. At this time, the β of S3', S4', and S5' were calculated to be 1.203×10^{-5} cm/W, 2.592×10^{-5} cm/W, and 2.447×10^{-5} cm/W respectively. As illustrated in Table 1, we compared the nonlinear absorption coefficients (β_{eff}) in relevant literatures with those in this work. The nonlinear absorption coefficient of Cu–Al–O thin films prepared in this paper is 10–10^6 times higher than that in relevant literatures [48–52]. The results show that the Cu–Al–O thin films not only realize nonlinear optical absorption conversion under the induction of thermal oxidation, but also have strong nonlinear absorption intensity, which can be used as excellent nonlinear optical materials.

The conversion of nonlinear saturable absorption to nonlinear reverse saturable absorption has been reported in many literatures and its conversion mechanism has been analyzed [53–55]. We proposed that under the combined action of oxygen defect, quantum confinement effect and multi-photon absorption, there existed the coexistence and competition between SA and RSA [56,57]. From the perspective of oxygen vacancy, the variation trend of nonlinear saturation absorption

Table 1
Comparison of the nonlinear absorption coefficient β_{eff} values in this work with those reported in the relevant literature.

Sample Material	Method	Wavelength (nm)	β_{eff} (cm/W)	References
Cu–Al–O thin film	PECVD	750	-1×10^{-6}	[9]
$Zn_{0.96}Cu_{0.04}Al_2O_4$	Combustion	532	1.4479×10^{-4}	[10]
$AgCu/Al_2O_3$ nanofilm	PLD&RTA	400	4.50×10^{-11}	[11]
$Cu_3Nb_2O_8$	Solid-state reaction	800	7.8×10^{-8}	[12]
ZnO–Cu	Colloidal chemical synthesis	532	2.938×10^{-11}	[13]
Cu–Al–O films	Magnetron sputtering	1550	2.592×10^{-5}	Present work

intensity of as-deposited Cu–Al–O films was basically consistent with that of oxygen vacancy. This is because the increase of oxygen vacancy leads to the increase of carrier concentration, which enhances the third-order nonlinear saturation absorption performance of the samples [30]. After thermal oxidation, due to the introduction of oxygen defects and the change of film surface structure [29], the saturation absorption intensity of the sample was further improved, see sample S2', where saturation absorption was dominant. Starting from the S3', the average particle size of the samples was less than 1 nm, which caused quantum confinement effect due to the small size effect, and it changed the electronic structure of nanocrystals and bulk materials [58]. As the size of the nanostructure decreased, the band gap of the semiconductor increased, accompanied by two-photon absorption or multi-photon absorption [59]. Therefore, the reverse from SA to RSA occurred, and the third order nonlinear absorption of the samples was dominated by reverse saturation absorption [17].

The finite difference time domain (FDTD) method is used to further investigate the effect of thermal oxidization on the electric field distribution of Cu–Al–O films, the results are shown in Fig. 7. In the simulation, a 1550 nm laser polarized along the y-axis incident vertically into the x-y plane of the samples. Fig. 7(a) represents the electric field distribution of the as-deposited Cu–Al–O film. It can be seen that the surface of the as-deposited films was smooth and compact, the electric field distribution was uniform, and the local electric field strength was 0.78. Fig. 7(b-d) show the simulated electric field distribution of the as-annealed samples S1', S2' and S3' with the local electric field intensity of 1.14, 1.3 and 1.9, respectively. After thermal treatment, the surface roughness of the films decreased, and the "hot spots" formed on the local surface between the nanoparticle spacing, resulting in enhanced electric fields. The results of FDTD show that the thermal treatment can effectively enhance the electric field intensity of the samples, thereby affecting the nonlinear absorption characteristics of the samples.

4. Conclusion

In summary, the Cu–Al–O thin films were fabricated by magnetron sputtering at room temperature, and the effects of thermal treatment on the structure and optical properties of the films were investigated. The existence of CuAlO2 phase and the increase of oxygen vacancy after thermal oxidation were confirmed by XPS analysis spectrum, which resulted in the blue-shift of characteristic absorption peak and the widening of band gap. According to the measurement results of nonlinear optics, the deposited Cu–Al–O films exhibited strong saturation absorption behavior. The nonlinear absorption mechanism of the as-annealed films changed from saturation absorption to reverse saturable absorption, and the nonlinear absorption coefficient (β) reached the maximum 2.592×10^{-5} cm/W. Therefore, Cu–Al–O films with excellent nonlinear absorption properties have potential applications in optical switching, optical limiter, and mode-locking.

CRediT authorship contribution statement

Jingjing Xu: Writing – original draft, Software. **Qingyou Liu:** Software. **Xiao Li:** Software. **Ruijin Hong:** Writing – review & editing, Supervision. **Chunxian Tao:** Data curation. **Qi Wang:** Data curation. **Hui Lin:** Formal analysis. **Zhaoxia Han:** Data curation. **Dawei Zhang:** Project administration, Validation.

Declaration of competing interest

The authors declare that they have no known competing financial interests or personal relationships that could have appeared to influence the work reported in this paper.

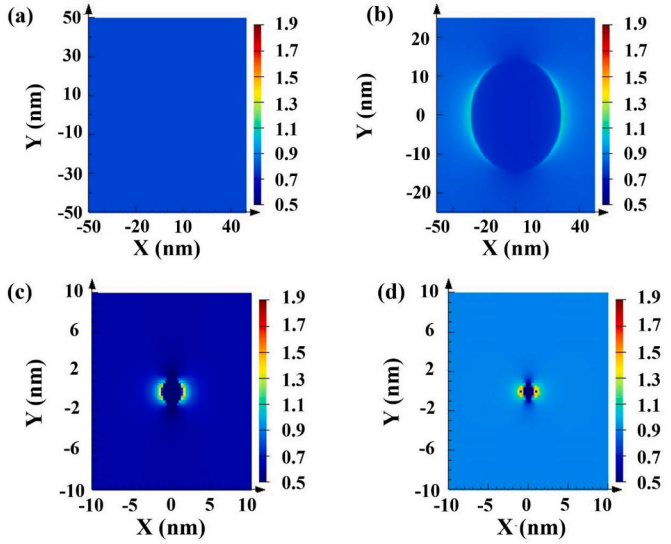

Fig. 7. FDTD simulated electric field amplitude patterns of **(a)** as-deposited Cu–Al–O film and as-annealed films **(b)** S1′, **(c)** S2′, **(d)** S3'.

Data availability

Data will be made available on request.

Acknowledgment

This work was supported by the National Natural Science Foundation of China (61775141, 62075133).

References

[1] H. Kawazoe, M. Yasukawa, H. Hyodo, M. Kurita, H. Yanagi, H. Hosono, P-type electrical conduction in transparent thin films of CuAlO2, Nature 389 (1997) 939–942.
[2] E.-B. Ko, J.-S. Choi, H. Jung, S.-C. Choi, C.-Y. Kim, Low temperature synthesis of fluorine-doped tin oxide transparent conducting thin film by spray pyrolysis deposition, J. Nanosci. Nanotechnol. 16 (2016) 1934–1937.
[3] H. Ohta, M. Orita, M. Hirano, I. Yagi, K. Ueda, H. Hosono, Electronic structure and optical properties of SrCu2O2, J. Appl. Phys. 91 (2002) 3074–3078.
[4] A. Banerjee, K. Chattopadhyay, Recent developments in the emerging field of crystalline p-type transparent conducting oxide thin films, Prog. Cryst. Growth Char. Mater. 50 (2005) 52–105.
[5] Z. Deng, X. Fang, R. Tao, W. Dong, D. Li, X. Zhu, The influence of growth temperature and oxygen on the phase compositions of CuAlO2 thin films prepared by pulsed laser deposition, J. Alloys Compd. 466 (2008) 408–411.
[6] T. Ehara, R. Iizaka, M. Abe, K. Abe, T. Sato, Preparation of CuAlO2 thin films by radio frequency magnetron sputtering and the effect of sputtering on the target surface, Journal of Ceramic Science Technology 8 (2017) 7–12.
[7] N. Benreguia, A. Barnabé, M. Trari, Sol–gel synthesis and characterization of the delafossite CuAlO2, J. Sol. Gel Sci. Technol. 75 (2015) 670–679.
[8] K. Vojisavljević, B. Malič, M. Senna, S. Drnovšek, M. Kosec, Solid state synthesis of nano-boehmite-derived CuAlO2 powder and processing of the ceramics, J. Eur. Ceram. Soc. 33 (2013) 3231–3241.
[9] G. Castillo-Hernández, S. Mayén-Hernández, E. Castaño-Tostado, F. DeMoure-Flores, E. Campos-González, C. Martínez-Alonso, J. Santos-Cruz, CuAlO2 and CuAl2O4 thin films obtained by stacking Cu and Al films using physical vapor deposition, Results Phys. 9 (2018) 745–752.
[10] P.-H. Hsieh, Y.-M. Lu, W.-S. Hwang, Effects of RF power on the growth behaviors of CuAlO2 thin films, Ceram. Int. 40 (2014) 9361–9366.
[11] H.-Y. Chen, J.-H. Ou, P-type transparent conductive CuAlO2 thin films prepared using atmospheric pressure plasma annealing, Mater. Lett. 228 (2018) 81–84.
[12] N. Tsuboi, Y. Takahashi, S. Kobayashi, H. Shimizu, K. Kato, F. Kaneko, Delafossite CuAlO2 films prepared by reactive sputtering using Cu and Al targets, J. Phys. Chem. Solid. 64 (2003) 1671–1674.
[13] H.-Y. Chen, M.-W. Tsai, Delafossite-CuAlO2 films prepared by annealing of amorphous Cu–Al–O films at high temperature under controlled atmosphere, Thin Solid Films 519 (2011) 5966–5970.
[14] L. Ma, C. Dong, W. Li, Q. Su, J. Zhou, E. Xie, W. Lan, Room-temperature power factor of CuAlO2 composite tablets enhanced by MWCNTs, Curr. Appl. Phys. 33 (2022) 27–32.

[15] H. Jiang, X. Zhu, H. Lei, G. Li, Z. Yang, W. Song, J. Dai, Y. Sun, Y. Fu, Effect of Cr doping on the optical–electrical property of CuAlO2 thin films derived by chemical solution deposition, Thin Solid Films 519 (2011) 2559–2563.
[16] N.S. Babu, Linear and nonlinear optical properties of ZnS/Ag2S composite nanoparticles, Mater. Today Proc. 45 (2021) 3976–3981.
[17] N.S. Babu, Nonlinear Optical Properties of Nanostructured Films of CdSe, Cu2Se and CdSe: Cu2Se, in: Materials Today: Proceedings, 2021.
[18] Y. Zu, C. He, D. Liu, L. Chen, W. Li, W. Zhang, Nonlinear optical properties of poly (vinyl alcohol) thin films doped with in-situ WSe2/rGO composite, Opt Laser. Technol. 142 (2021), 107198.
[19] M. Fang, H. He, B. Lu, W. Zhang, B. Zhao, Z. Ye, J. Huang, Optical properties of p-type CuAlO2 thin film grown by rf magnetron sputtering, Appl. Surf. Sci. 257 (2011) 8330–8333.
[20] A.S. Reddy, H.-H. Park, G.M. Rao, S. Uthanna, P.S. Reddy, Effect of substrate temperature on the physical properties of dc magnetron sputtered CuAlO2 films, J. Alloys Compd. 474 (2009) 401–405.
[21] A. Panthawan, T. Kumpika, W. Sroila, E. Kantarak, W. Thongpan, P. Pooseekheaw, R. Sornphanpee, N. Jumrus, P. Sanmuangmoon, A. Tuantranont, Morphology and phase transformation of copper/aluminium oxide films, Ukrainian J. Phys. 63 (2018), 425-425.
[22] R.-S. Yu, C.-J. Lu, D.-C. Tasi, S.-C. Liang, F.-S. Shieu, Phase transformation and optoelectronic properties of p-type CuAlO2 thin films, J. Electrochem. Soc. 154 (2007) H838.
[23] I.Y. Bu, Optoelectronic properties of novel amorphous CuAlO2/ZnO NWs based heterojunction, Superlattice. Microst. 60 (2013) 160–168.
[24] J. Cai, H. Gong, The influence of Cu/ Al ratio on properties of chemical-vapor-deposition-grown p-type Cu–Al–O transparent semiconducting films, J. Appl. Phys. 98 (2005), 033707.
[25] J. Pan, Y. Sheng, J. Zhang, P. Huang, X. Zhang, B. Feng, Photovoltaic conversion enhancement of a carbon quantum dots/p-type CuAlO2/n-type ZnO photoelectric device, ACS Appl. Mater. Interfaces 7 (2015) 7878–7883.
[26] L. Hao, Y. Toyama, N. Feng, Y. Jin, Y. Lu, Synergetic improvement strategy on thermoelectric performance of CuAlO2 compacts, Ceram. Int. 45 (2019) 5486–5490.
[27] B. Zhang, M. Cheng, G. Liu, Y. Gao, L. Zhao, S. Li, Y. Wang, F. Liu, X. Liang, T. Zhang, Room temperature NO2 gas sensor based on porous Co3O4 slices/ reduced graphene oxide hybrid, Sensor. Actuator. B Chem. 263 (2018) 387–399.
[28] N. Daichakomphu, A. Harnwunggmoung, N. Chanlek, R. Sakdanuphab, A. Sakulkalavek, Figure of merit improvement of delafossite CuAlO2 with the addition of Fe and graphene, J. Phys. Chem. Solid. 134 (2019) 29–34.
[29] Z. Zhao, T. Jia, J. Lin, Z. Wang, Z. Sun, Femtosecond non-resonant optical nonlinearity of silver chloride nanocrystal doped niobic tellurite glass, J. Phys. Appl. Phys. 42 (2009), 045107.
[30] H. Yin, Y. Zhao, J. Li, Q. Yang, W. Wu, Optical and electrical properties of Ag: Cu2O nanocomposite films prepared by pulse laser deposition, Mater. Chem. Phys. 241 (2020), 122399.
[31] H. Akyildiz, Synthesis of CuAlO2 from chemically precipitated nano-sized precursors, Ceram. Int. (2015) 14108–14115.
[32] J. Ding, Y. Sui, W. Fu, H. Yang, S. Liu, Y. Zeng, W. Zhao, P. Sun, J. Guo, H. Chen, Synthesis and photoelectric characterization of delafossite conducting oxides CuAlO2 laminar crystal thin films via sol–gel method, Appl. Surf. Sci. 256 (2010) 6441–6446.
[33] T. Suriwong, T. Thongtem, S. Thongtem, Thermoelectric and optical properties of CuAlO2 synthesized by direct microwave heating, Curr. Appl. Phys. 14 (2014) 1257–1262.
[34] N. Daichakomphu, B. Klongratog, P. Rodpun, P. Pluengphon, A. Harnwunggmoung, Y. Poo-arporn, A. Sakulkalavek, R. Sakdanuphab, Improving the photo-thermoelectric performance of CuAlO2 via doping with Bi, Mater. Res. Bull. 144 (2021), 111479.
[35] M. Balık, V. Bulut, I.Y. Erdogan, Optical, structural and phase transition properties of Cu2O, CuO and Cu2O/CuO: their photoelectrochemical sensor applications, Int. J. Hydrogen Energy 44 (2019) 18744–18755.
[36] J.I. Pankove, Optical Processes in Semiconductors, vol. 92, Prentice-Hall, New Jersey, 1971, p. 36.
[37] I. Jacques, Pankove, Optical Processes in Semiconductors, Dover publication institute, New York, 1971.
[38] M. Nisha, S. Anusha, A. Antony, R. Manoj, M. Jayaraj, Effect of substrate temperature on the growth of ITO thin films, Appl. Surf. Sci. 252 (2005) 1430–1435.
[39] Y. Jo, C. Hong, J. Kwak, Improved electrical and optical properties of ITO thin films by using electron beam irradiation and their application to UV-LED as highly transparent p-type electrodes, Curr. Appl. Phys. 11 (2011) S143–S146.
[40] A. Banerjee, K. Chattopadhyay, Size-dependent optical properties of sputter-deposited nanocrystalline p-type transparent Cu Al O 2 thin films, J. Appl. Phys. 97 (2005), 084308.
[41] C. Lu, H. Xuan, Y. Zhou, X. Xu, Q. Zhao, J.J.P.R. Bai, Saturable and Reverse Saturable Absorption in Molybdenum Disulfide Dispersion and Film by Defect Engineering, vol. 8, 2020, pp. 1512–1521.
[42] M. Zhao, P. Song, J. Teng, Interfaces, electrically and optically tunable responses in graphene/transition-metal-dichalcogenide heterostructures, ACS Appl. Mater. Interfaces 10 (2018) 44102–44108.
[43] B.G. Shetty, V. Crasta, N.R. Kumar, K. Rajesh, R. Bairy, Effect of nano fillers on electrical, mechanical, fluorescent and third order nonlinear optical properties of PVA, Mater. Res. Express 6 (2019), 75055.
[44] K. Nagaraja, S. Pramodini, P. Poornesh, H. Nagaraja, Effect of annealing on the structural and nonlinear optical properties of ZnO thin films under cw regime, J. Phys. Appl. Phys. 46 (2013), 55106.
[45] Z. Li, R. Hong, Q. Liu, Q. Wang, C. Tao, H. Lin, D. Zhang, Laser patterning induced the tunability of nonlinear optical property in silver thin films, Chem. Phys. Lett. 751 (2020), 137535.
[46] M. Banuprakash, B. Abhishek, H. Acharya, R. Bairy, S. Bhat, H. Vijeth, M. Murari, A. Jayarama, R. Pinto, Structural, linear and nonlinear optical characterization of Ni and Al Co-Doped CdO semiconductor nanostructures for nonlinear optical device applications, in: Materials Today: Proceedings, 2021, pp. 396–404, 35.
[47] R. Bairy, P. shankaragouda Patil, S.R. Maidur, H. Vijeth, M. Murari, U. Bhat, The role of cobalt doping in tuning the band gap, surface morphology and third-order optical nonlinearities of ZnO nanostructures for NLO device applications, RSC Adv. 9 (2019) 22302–22312.
[48] C. Wen, Optical and Mechanical Properties of Cu-Al-O Thin Films Prepared by Plasma-Enhance CVD, 2005.
[49] P. Surendran, A. Lakshmanan, S.S. Priya, K. Balakrishnan, T.A. Hegde, G. Vinitha, G. Ramalingam, P. Rameshkumar, K. Kaviyarasu, Optical and nonlinear optical properties of Zn0. 96Cu0. 04Al2O4 nanocomposites prepared by combustion method, in: Materials Today: Proceedings, 2021, pp. 175–178, 36.
[50] X. Gao, C. Zou, H. Zhou, C. Yuan, J. He, X. Luo, Enhanced nonlinear optical properties of alloyed AgCu glassy nanoparticles, J. Alloys Compd. 819 (2020), 153003.
[51] N. Priyadarshani, T.S. Girisun, S.V. Rao, Improved femtosecond third-order nonlinear optical properties of thin layered Cu3Nb2O8, Opt. Mater. 88 (2019) 586–593.
[52] L. Irimpan, V. Nampoori, P. Radhakrishnan, Enhanced luminescence and nonlinear optical properties of nanocomposites of ZnO–Cu, J. Mater. Res. 23 (2008) 2836–2845.
[53] S. Mirershadi, S. Ahmadi-Kandjani, A. Zawadzka, H. Rouhbakhsh, B. Sahraoui, Third order nonlinear optical properties of organometal halide perovskite by means of the Z-scan technique, Chem. Phys. Lett. 647 (2016) 7–13.
[54] K. Iliopoulos, A. El-Ghayoury, B. Derkowska, A. Ranganathan, P. Batail, D. Gindre, B. Sahraoui, Effect of the counter cation on the third order nonlinearity in anionic Au dithiolene complexes, Appl. Phys. Lett. 101 (2012), 261105.
[55] K. Iliopoulos, A. El-Ghayoury, H. El Ouazzani, M. Pranaitis, E. Belhadj, E. Ripaud, M. Mazari, M. Sallé, D. Gindre, B. Sahraoui, Nonlinear absorption reversing between an electroactive ligand and its metal complexes, Opt Express 20 (2012) 25311–25316.
[56] K. Wang, H. Long, M. Fu, G. Yang, P. Lu, Intensity-dependent reversal of nonlinearity sign in a gold nanoparticle array, Opt. Lett. 35 (2010) 1560–1562.
[57] K. Wang, H. Long, M. Fu, G. Yang, P. Lu, Size-related third-order optical nonlinearities of Au nanoparticle arrays, Opt Express 18 (2010) 13874–13879.
[58] Q. Wan, C. Lin, N. Zhang, W. Liu, G. Yang, T. Wang, Linear and third-order nonlinear optical absorption of amorphous Ge nanoclusters embedded in Al2O3 matrix synthesized by electron-beam coevaporation, Appl. Phys. Lett. 82 (2003) 3162–3164.
[59] L. Polavarapu, N. Venkatram, W. Ji, Q.-H. Xu, Optical-limiting properties of oleylamine-capped gold nanoparticles for both femtosecond and nanosecond laser pulses, ACS Appl. Mater. Interfaces 1 (2009) 2298–2303.